Engineering Structures 65 (2014) 76–88

Contents lists available at ScienceDirect

Engineering Structures

journal homepage: www.elsevier.com/locate/engstruct

Influence of boundary conditions and size effect on the drift capacity of URM walls

Sarah Petry, Katrin Beyer *

[a] Earthquake Engineering and Structural Dynamics Laboratory (EESD), School of Architecture, Civil and Environmental Engineering (ENAC), École Polytechnique Fédérale de Lausanne (EPFL), EPFL ENAC IIC EESD, GC B2 515, Station 18, CH – 1015 Lausanne, Switzerland

ARTICLE INFO

Article history:
Received 21 August 2013
Revised 18 December 2013
Accepted 29 January 2014

Keywords:
Unreinforced masonry
Drift capacity
Boundary conditions
Size effects
Quasi-static cyclic tests
Walls

ABSTRACT

In codes the drift capacity of unreinforced masonry (URM) walls is often estimated as a function of the failure mode and the aspect ratio. The empirical relationships are based on results from quasi-static cyclic tests on single URM walls, which were tested simulating either fixed-fixed or cantilever boundary conditions. In real structures, the stiffness and strength of slabs and spandrels define the boundary conditions of the walls and therefore the moment, shear force and axial force imposed on a wall during an earthquake. Depending on the exact configuration of wall, slab and spandrel, the boundary conditions can vary significantly.

In order to investigate the influence of these boundary conditions on the force-deformation behaviour of URM walls, six quasi-static cyclic tests were performed. Different boundary conditions were simulated by varying the axial load ratio and the ratio of top and bottom moment applied to the wall. This article presents the test results and discusses the influence of the boundary conditions on the failure mechanism and the drift capacity of the walls. In addition, the results from 64 quasi-static tests on URM walls of different heights and masonry types are evaluated. These tests confirm the influence of the boundary conditions on the drift capacity. Moreover, they show that a strong size effect is present which leads to smaller drift capacities with increasing wall height. For this reason, an empirical drift capacity equation is proposed which accounts for the moment profile, the axial load ratio and the size effect.

1. Introduction

In unreinforced masonry (URM) buildings, walls are connected by horizontal structural elements such as slabs and masonry spandrels. When walls are subjected to in-plane loading, these horizontal elements act as coupling elements between the walls and the system is often analysed using equivalent frame models [1]. The stiffness and strength of these coupling elements can vary significantly and three levels of coupling are distinguished in the literature, see Fig. 1, e.g. [2,3]: (i) weak coupling, where the horizontal elements impose only equal displacements on the walls of each storey but do not transfer significant shear forces or bending moments, (ii) strong coupling, where vertical and horizontal elements develop together a framing action and where the coupling elements remain largely elastic when the structure is subjected to horizontal loading, (iii) intermediate coupling, where the moments transferred by the coupling elements are limited but not negligible. The coupling elements influence the rotational restraint at the top of the wall and therefore, the moment profile. For outer walls, the coupling elements cause also a variation of axial force in the wall. For inner walls in symmetrical structures, the axial force variation due to the horizontal loading is small and can often be neglected.

In most codes, such as EC8-Part 3 [4], the drift capacity of URM walls is estimated as a function of the failure mode and the aspect ratio. These empirical relationships are based on results from quasi-static cyclic tests on URM walls, which were tested simulating either fixed-fixed or cantilever conditions. Hence, as only two types of boundary conditions were applied, a detailed investigation on the influence of the boundary conditions on displacement capacities of URM walls was not possible. To complement previous tests, this study comprises six wall tests with different boundary conditions typical for internal or external walls in URM buildings with RC slabs. The findings are compared to the results of a dataset comprising 64 wall tests and the relationship between axial stress, degree of coupling and displacement capacity is discussed. The dataset also shows that the displacement capacity of URM walls is affected by a strong size effect: tests on walls with smaller height lead to higher drift capacities than full storey height walls. New equations for drift capacity should therefore account for the

* Corresponding author. Tel.: +41 21 6936234; fax: +41 21 693 57 00.
E-mail addresses: sarah.petry@epfl.ch (S. Petry), katrin.beyer@epfl.ch (K. Beyer).

http://dx.doi.org/10.1016/j.engstruct.2014.01.048
0141-0296/

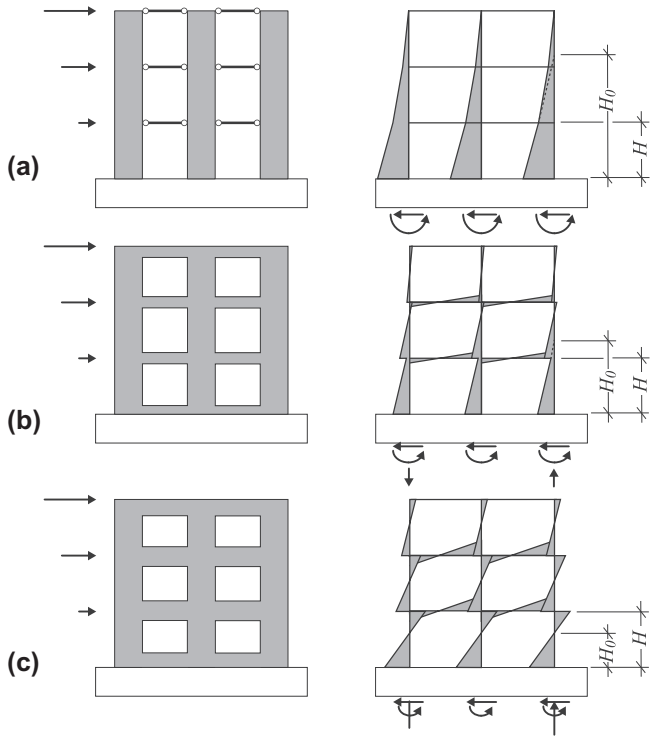

Fig. 1. Moment profiles of masonry wall structures with (a) weak coupling, (b) intermediate coupling and (c) strong coupling, taken from [3].

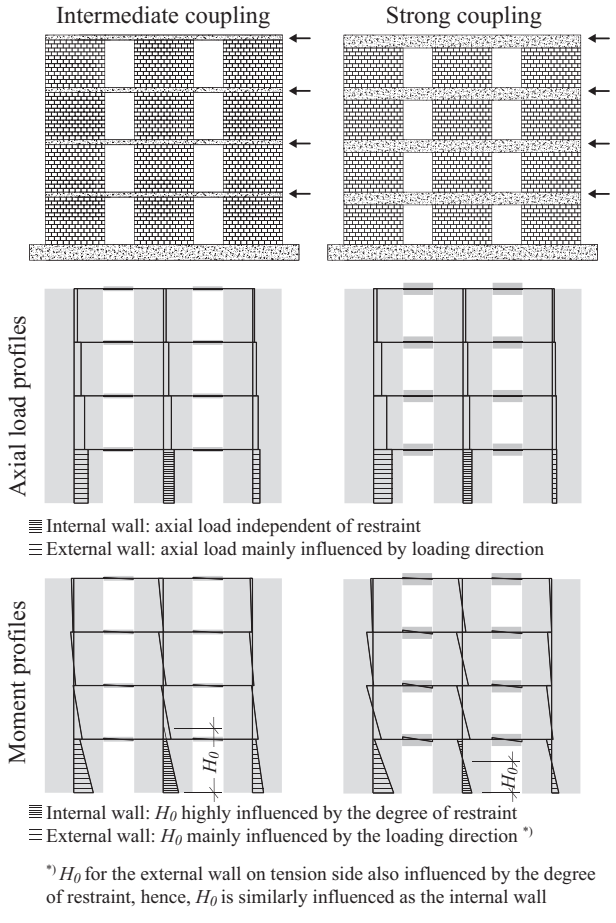

Fig. 2. Results from a pushover analyses on URM-wall structures with intermediate coupling (left) and strong coupling (right).

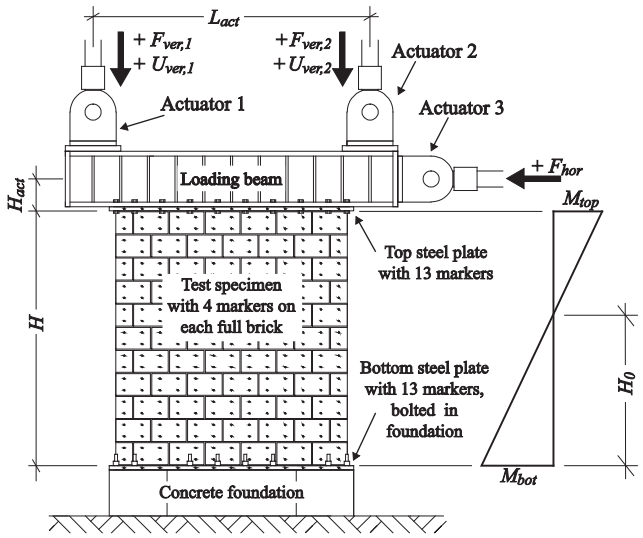

Fig. 3. Drawing of EPFL test stand.

Fig. 4. Photo of EPFL test stand.

boundary conditions (moment profile, axial load ratio) and the size effect.

2. Quasi-static cyclic tests on masonry walls

To investigate the effect of the boundary conditions (axial load ratio and moment profile) on the deformation capacity of URM walls, a series of six wall tests was designed. The boundary conditions to be applied in the tests were derived from pushover analyses of a 4-storey masonry wall with RC slabs using the macro-element program Tremuri [1,5]. The wall was analysed for

Table 1
Boundary conditions of PUP1-6.

Specimen	Wall	Normal stress level	σ_0/f_u	Degree of coupling	Shear span H_0
PUP1	Internal	Intermediate	0.18	Strong	0.5*H*
PUP2	Internal	Intermediate	0.18	Strong	0.75*H*
PUP3	Internal	Intermediate	0.18	Intermediate	1.5*H*
PUP4	External	High	0.26	Intermediate	1.5*H*
PUP5	External	Low	0.09	Strong	0.75*H*
PUP6	External	High	0.26	Intermediate	1.5*H*
		Low	0.09	Strong	0.75*H*

two different moment capacities of the RC beam elements representing a case of intermediate coupling (Fig. 2 left) and strong coupling (Fig. 2 right).

The walls were tested using the test stand shown in Figs. 3 and 4. The test stand allowed applying one horizontal force and two vertical forces by means of three servo-hydraulic actuators, which were controlled in a fully coupled mode. All six walls had the same height H, length L and thickness T (H = 2.25 m, L = 2.01 m, T = 0.20 m). The first three tests (PUP1-3) simulated an internal wall and the next three tests (PUP4-6) an external wall. All tests represented walls at the first floor where failure in URM buildings is expected. The following section summarises the analysis results and the boundary conditions derived for the tests.

2.1. Simulating the boundary conditions of internal walls: PUP1 to PUP3

In URM buildings with a regular wall layout, the axial force in an internal wall does not vary significantly when the wall is subjected to horizontal loading. Hence, the axial load in internal walls can be assumed independent from the degree of coupling and only the rotational top restraint was changed between PUP1-3. For the 4-storey reference building, the axial load acting on an internal wall at the ground floor is N = 419 kN. This corresponds to a normal stress ratio of σ_0/f_u = 0.18, where f_u represents the average compressive strength of the investigated masonry and σ_0 the applied normal stress.

2.1.1. Reference test specimen PUP1

For the first test specimen PUP1 standard fixed-fixed boundary conditions were applied, i.e., the rotation of the top beam was controlled to be zero, while the total normal force was kept constant:

$$N = F_{ver,1} + F_{ver,2} = \text{constant} \tag{1}$$

where N is the total normal load and $F_{ver,1}$ and $F_{ver,2}$ the force applied through the two vertical actuators (see Fig. 3).

2.1.2. Reduced rotational top constraints for PUP2 and PUP3

The effect of different degrees of coupling on the axial load and moment profiles is shown in Fig. 2. It can be seen that fixed-fixed boundary conditions are not representative for the moment profiles over the height of an internal wall of the first storey. For most building configurations, the bottom moment of the wall is significantly larger than the top moment. For weak to intermediate coupling, the top and bottom moment might even have the same sign. Thus, PUP2 and PUP3 were allowed a limited top rotation. Instead of controlling this top rotation, the height of the shear span H_0 was kept constant throughout the test, i.e., the applied moment at the top was a function of the applied horizontal force. The total axial load applied by the two vertical actuators was maintained constant throughout the test. For PUP2 and PUP3, the shear span was fixed at H_0 = 0.75H and 1.5H, respectively, where H is the height of the wall (Table 1).

2.2. Simulating the boundary conditions of an external wall: PUP4 to PUP6

2.2.1. PUP4 and PUP5 with constant axial load and constant shear span

In an external wall, a unilateral coupling moment is introduced and affects thus the axial load in the wall. Fig. 2 shows that the axial load in an outer wall at the first storey fluctuates by approximately ±50%. Hence, PUP4 and PUP5 were tested under a constant axial load of 619 kN and 219 kN, respectively. However, with varying axial force also the shear span changed (Fig. 2) and therefore for PUP4 and PUP5 shear spans of H_0 = 0.75H and 1.5H were chosen, respectively (Table 1).

2.2.2. Varying axial load and shear span for PUP6

In a real building, the axial load in an external wall varies with the direction of the lateral load. While for one loading direction the axial load in the wall increases, it decreases for the opposite loading direction (see Fig. 2). Hence, when simulating an external wall, the boundary conditions applied to PUP4 and PUP5 should be combined. Therefore for PUP6, the axial load and shear span were taken as linear functions of the horizontal load F_{hor}. Hence, the boundary conditions of PUP6 approached in the negative and positive directions, those of PUP4 and PUP5, respectively:

$$N = \frac{N_{\max} + N_{\min}}{2} - F_{hor} \cdot \frac{N_{\max} - N_{\min}}{F_{\text{hor,max}} - F_{\text{hor,min}}} \tag{2}$$

$$H_0 = \frac{H_{0,\min} + H_{0,\max}}{2} - F_{hor} \cdot \frac{H_{0,\max} - H_{0,\min}}{F_{\text{hor,max}} - F_{\text{hor,min}}} \tag{3}$$

where $N_{\max}$ = 619 kN, $N_{\min}$ = 219 kN, $H_{0,\min}$ = 0.75H and $H_{0,\max}$ = 1.5H correspond to the boundary conditions of PUP4 and PUP5, while $F_{hor,\max} = -F_{hor,\min}$ = 133 kN was determined as the average of the horizontal force capacities obtained from PUP4 and PUP5.

2.3. Instrumentation and testing procedure

A set of conventional hard-wired measurements was used to measure the forces in all three actuators, the displacement at the top of the wall and local deformations in bricks and joints at all four corners of the wall. In addition, a LED-based optical measurement system was used to follow the displacements of the wall and at the steel plates at the top and bottom of the wall (see markers in Fig. 3). The force-drift hystereses in Figs. 6–11c were obtained from the average displacement of the markers on the top steel plate. Note that the drift herein this article stands for the interstorey drift, which is obtained when dividing the top displacement by the height of the walls. In the reinforced concrete community, the drift is often defined as chord rotation which is computed as the displacement at the inflection point divided by the shear span. While for walls tested as cantilever or under fixed-fixed boundary conditions chord rotation and interstorey are the same, they diverge from each other for walls tested under different boundary conditions. From our own tests, which included tests with shear span ratios different to 1 or 0.5, we found that interstorey drift approximates chord rotation in general reasonably well. The ratio of interstorey drifts to chord rotations are approximately 1.05 for H_0/H = 0.75 and 0.85 for H_0/H = 1.5.

After applying the axial load, the test unit was subjected to drift cycles with the following amplitudes: 0.025%, 0.05%, 0.1%, 0.15%, 0.2%, 0.3%, 0.4%, 0.6%, 0.8% and 1.0% (see Fig. 5). Note that the cycles with amplitudes of 0.15% and 0.25% were not included in the loading history applied to PUP1, but added from PUP2 onwards since

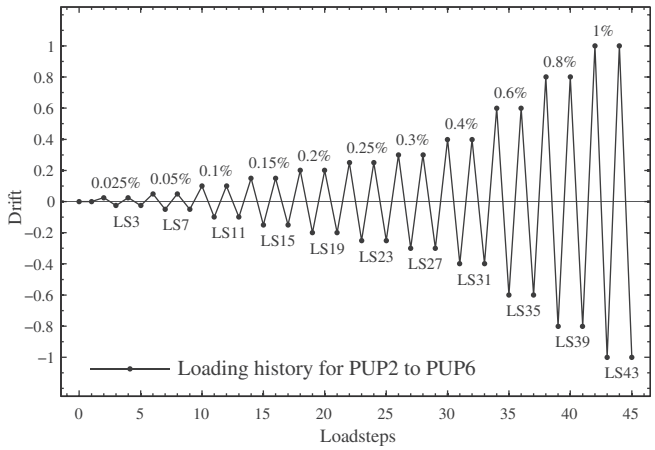

Fig. 5. Loading history for walls PUP2-6. For PUP1 the cycles with amplitudes of 0.15% and 0.25% were not applied.

the performance of PUP1 deteriorated rapidly within the cycles with amplitudes of 0.2% and 0.3%.

3. Material properties

The walls were constructed with a typical modern Swiss hollow clay brick unit. The head and bed joints were fully mortared and were 10–12 mm thick. The outer dimensions of the bricks were 190 × 300 × 195 mm ($H \times L \times W$). Webs and shells were 8–10 mm thick and the void ratio was 49%. The mean strength values and coefficients of variation obtained from material tests on the bricks are summarized in Table 2. The cement mortar WEBER MUR MAXIT 920, used for the construction of the walls, is one of the most commonly used mortars in Switzerland. Mortar samples were taken while constructing walls and wallettes for material tests. The mortar samples were tested as the same time as the corresponding walls and wallettes. The mortar properties are summarized in Table 2.

To determine the material properties of the masonry, three types of standard material tests were conducted: (i) 5 compression tests on masonry wallettes [6], (ii) 8 shear tests on masonry triplets [7] and (iii) 5 diagonal tensile tests on square masonry wallettes [8]. The results are summarized in Table 3.

4. Results from wall tests

For all test units, the loading was continued until the walls were no longer able to carry the applied vertical load. Therefore, within this series, two different failure limit states are distinct: (i) the horizontal load failure is defined as the drift where the strength dropped to 80% of the peak strength and (ii) the vertical load failure is attained, when the walls can no longer sustain the load applied by the vertical pistons. The horizontal failure corresponds to the limit state "Near Collapse" as defined in EC8-Part 3 [4]. Figs. 6–11 show the crack pattern of PUP1-6 after horizontal and vertical load failure, the applied boundary conditions and the hysteretic response. The following sections discuss the influence of the shear span, the axial load ratio and the loading history on the deformation behaviour of the test units.

Table 2
Brick and mortar properties.

Brick strength:		
Compression, ‖ to perforation	35.0 ± 7%	MPa
Compression, ⊥ to perforation	9.4 ± 8%	MPa
Flexural tensile, ⊥ to perforation	1.27 ± 38%	MPa
Mortar properties:		
Compression strength	11.2 ± 20%	MPa
Flexural tensile strength	2.7 ± 25%	MPa

Table 3
Masonry properties.

Results from compression tests:		
Compression strength f_u	5.87 ± 5%	MPa
E-modulus E	3550 ± 9%	MPa
Poisson ratio ϑ	0.20 ± 19%	–
Results from shear tests:		
Peak strength τ_{peak}	$0.94\sigma + 0.27$	MPa
Residual strength τ_{res}	0.91σ	
Results from diagonal tensile tests:		
Diagonal tensile strength	0.50 ± 10%	MPa

4.1. Influence of the shear span H_0

PUP1-3 were tested under the same constant average normal stress but the three tests differed with respect to the applied shear span ratio (PUP1: $H_0/H = 0.5$, PUP2: $H_0/H = 0.75$, PUP3: $H_0/H = 1.5$). PUP1 and PUP2 developed a shear failure while PUP3 failed due to rocking. All three walls developed first horizontal cracks in the mortar joints. While horizontal cracks appeared simultaneously at the top and bottom of PUP1, the horizontal joints at the top of PUP2 and PUP3 remained almost uncracked due to the smaller top moment. The horizontal cracks at the base of PUP2 and PUP3, however, opened up wider and spread over a larger height than in PUP1. In PUP1 and PUP2 the first diagonal cracks appeared at a nominal drift of 0.1%. Differences could be observed with regard to the initial inclination of the diagonal cracks, which were steeper for PUP2 (30-35° with respect to the vertical, Fig. 7a) than for PUP1 (cracks followed from the beginning the diagonal of the wall, Fig. 6a). With continuing loading and degradation, further inclined cracks developed in PUP2 and finally, the deformations concentrated along one diagonal crack spanning from one corner of the wall to the other, similar to PUP1 (compare Fig. 7a and b). In PUP3, the first inclined cracks appeared not before the cycles with a nominal drift of 0.4% and did not influence the failure mode (see Fig. 8a and b). When comparing the displacement capacity of PUP1-3 (see Table 4), it can be noticed that the capacity increased with increasing shear span. This applied to the displacement capacity associated with horizontal as well as vertical load failure. The increased displacement capacity was mainly due to the increased flexural deformations of the walls: while in PUP1 only few horizontal cracks developed at the top and bottom of the wall before deformations concentrated in one diagonal crack, horizontal cracking in PUP2 and PUP3 spread over a larger portion of the wall. An increased shear span leads therefore to an increase in deformation capacity.

4.2. Effect of the axial load ratio σ_0/f_u

PUP2 and PUP5 were both tested applying a constant shear span of $0.75H$. The two test units differed with respect to the applied axial load (PUP2: $\sigma_0/f_u = 0.18$, PUP5: $\sigma_0/f_u = 0.09$). Both walls showed at the beginning a similar crack pattern: the first cracks were horizontal cracks at the base of the wall. Shortly after, the first diagonal cracks appeared (at a nominal drift of 0.1% for PUP2 and 0.15% for PUP5). In both cases the first diagonal crack was steeper than the dominating crack at failure (see Figs. 7 and 10a and b). However, the larger normal force of PUP2 seemed to provoke more inclined cracks through the bricks, while in PUP5 the inclined cracks followed at the beginning the joints (stair step cracks) and passed only later through the bricks leading to a smaller strength

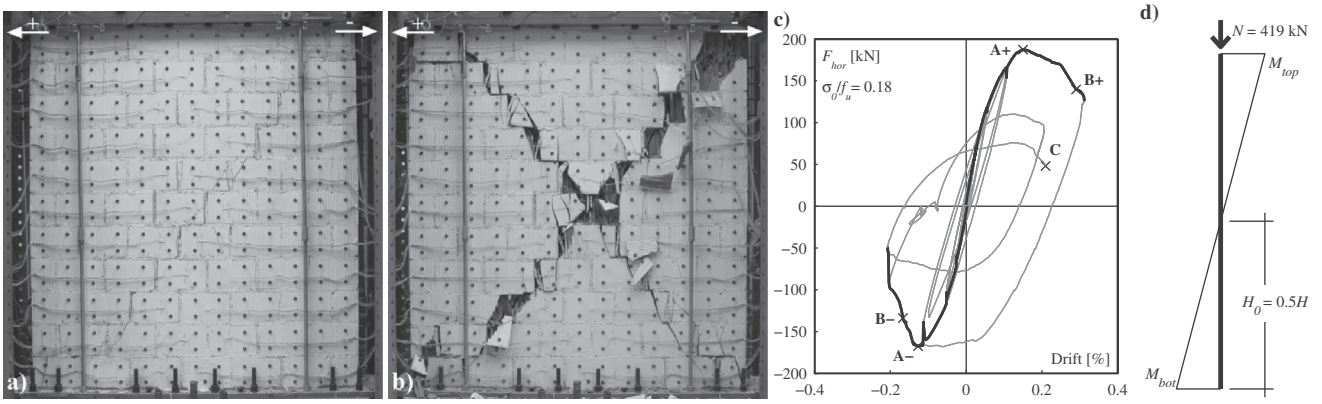

Fig. 6. PUP1: (a) after reaching the horizontal failure (B+), (b) after vertical failure (C), (c) interstorey drift-force hysteresis and (d) moment diagram.

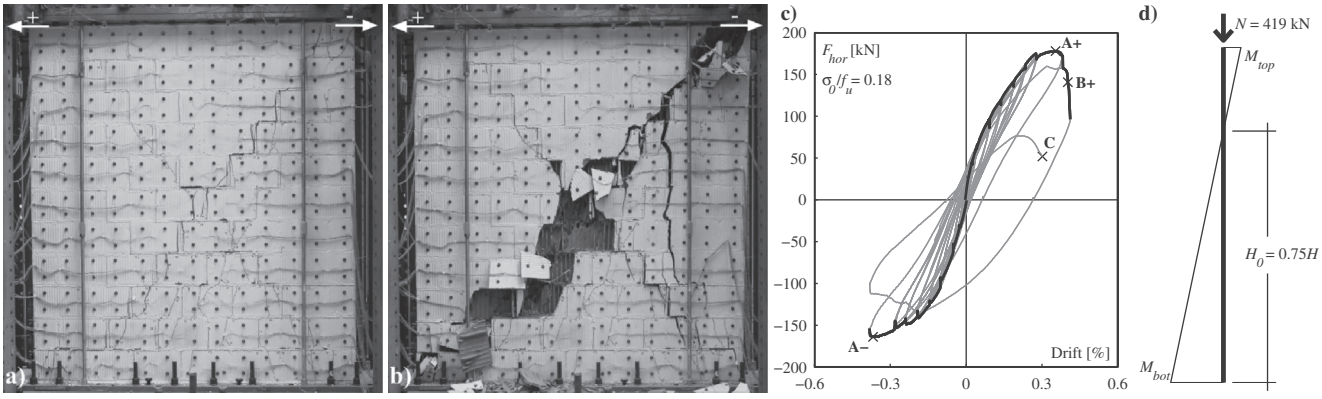

Fig. 7. PUP2: (a) after reaching the horizontal failure (B+), (b) after vertical failure (C), (c) interstorey drift-force hysteresis and (d) moment diagram.

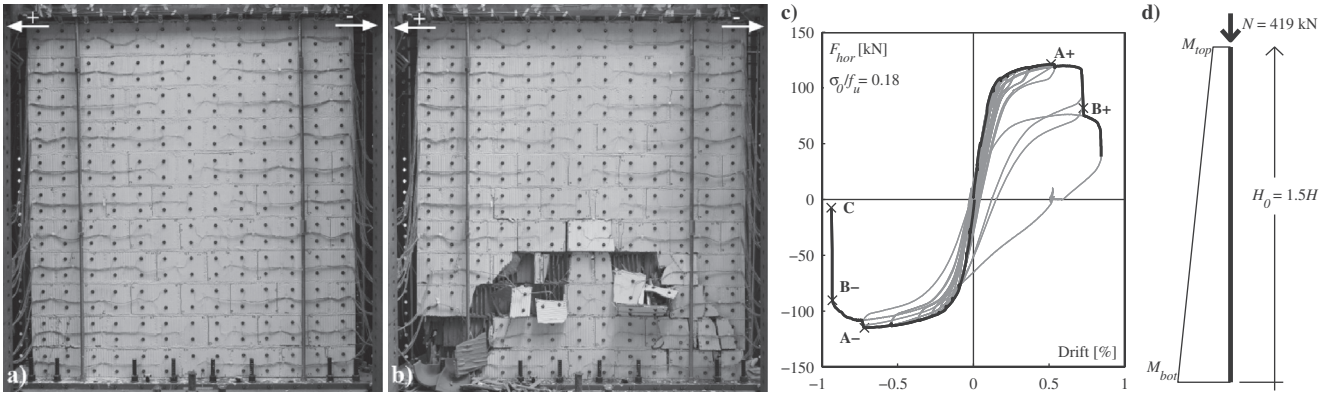

Fig. 8. PUP3: (a) after reaching the horizontal failure (B+), (b) after vertical failure (C), (c) interstorey drift-force hysteresis and (d) moment diagram.

degradation than for PUP2. Although both test units developed a shear failure mode, the displacement capacity of PUP5 was approximately 40% larger than the one of PUP2 (this applied to horizontal load failure and vertical load failure). It is assumed that the reduced degradation of the diagonal crack increased the displacement capacity for PUP5 (see Table 4).

Also PUP3 and PUP4 were both tested with a constant shear span of 1.5H and differed with respect to the applied axial load (PUP3: $\sigma_0/f_u = 0.18$, PUP4: $\sigma_0/f_u = 0.26$). Both walls developed first a flexural behaviour, while inclined cracks formed only at a later stage. PUP3 and PUP4 failed eventually due to a flexural and a hybrid failure, respectively. Due to the higher level of normal stresses and shear stresses in PUP4, the inclined cracks and local crushing at the toe appeared for PUP4 at smaller displacement demands than for PUP3 (see Table 4) leading to a faster strength degradation of PUP4. Thus, similar to PUP2/PUP5, the increase in axial load led to a reduced drift capacity.

4.3. Asymmetrical loading

The boundary conditions of PUP6 approached for the positive loading direction those of PUP5 and for the negative loading direction those of PUP4. Figs. 12 and 13 show the applied axial load and shear span ratio as function of the applied horizontal load and drift. The critical loading direction of PUP6 was the negative direction where the boundary conditions of PUP4 were approached. For

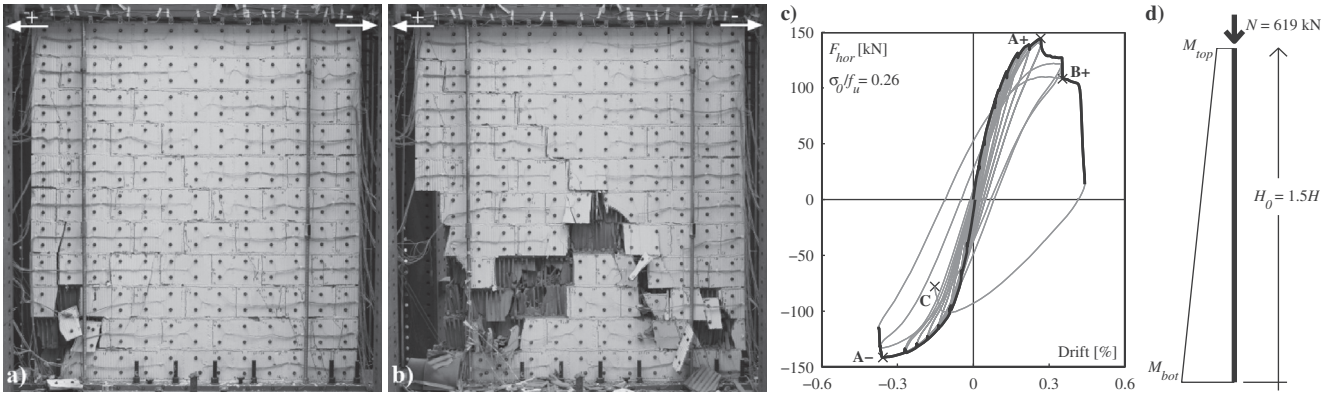

Fig. 9. PUP4: (a) after reaching the horizontal failure (B+), (b) after vertical failure (C), (c) interstorey drift-force hysteresis and (d) moment diagram.

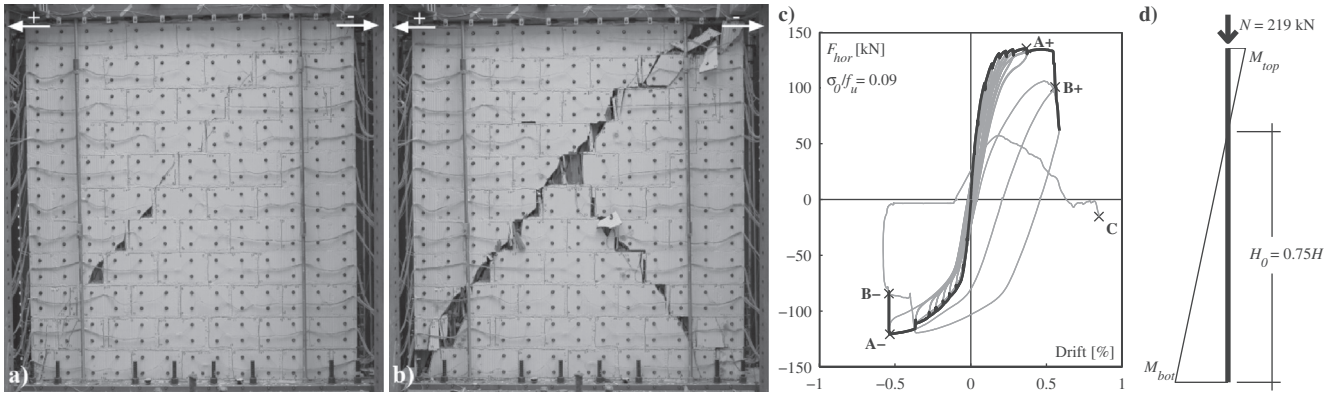

Fig. 10. PUP5: (a) after reaching the horizontal failure (B+), (b) after vertical failure (C), (c) interstorey drift-force hysteresis and (d) moment diagram.

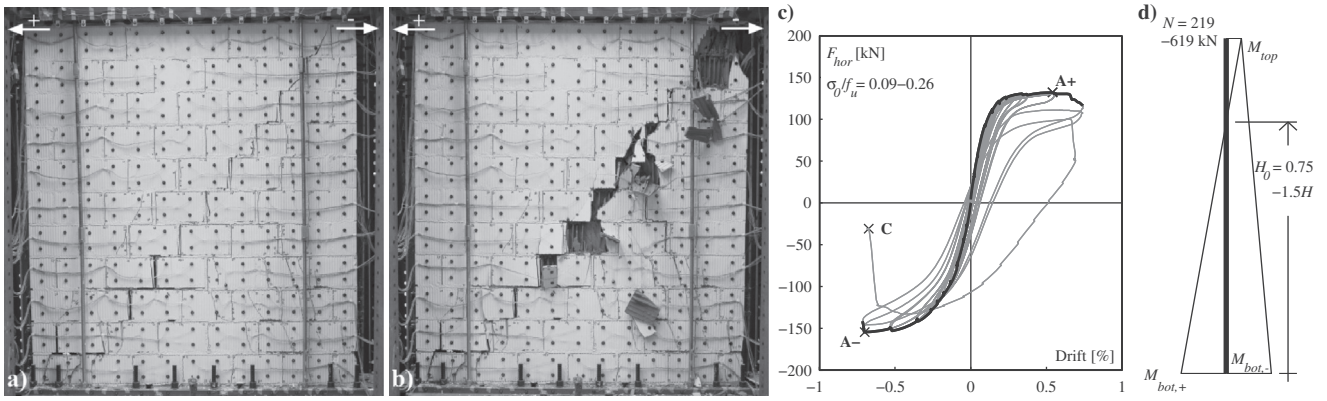

Fig. 11. PUP6: (a) after strength deterioration (~A+), (b) after vertical failure (C), (c) interstorey drift-force hysteresis and (d) moment diagram.

horizontal and vertical load failure, the drift capacities of PUP6 were 2.0 and 1.6 times larger than those of PUP4 (Table 4), i.e. the results suggest that the displacement capacity of symmetrical loaded walls is smaller than the displacement capacities of walls that are asymmetrically loaded and do not reach failure for one of the loading directions.

5. Empirical models for the drift capacity of URM walls

Deformation-based seismic assessment methods for URM structures require as input parameter estimates of the drift capacity of URM walls. The objective of this section is to review existing drift estimates for URM walls by comparing these to a dataset of 64 walls (Table 5). Hereinafter, the term drift capacity refers to the minimum drift capacity associated with horizontal load failure. If the horizontal failure was not measured before vertical failure was reached, the maximum drift is taken (see bold values in Table 4).

5.1. Drift capacity models in codes

The Eurocode, the Italian, New Zealand and Swiss code as well as several FEMA guidelines include drift capacity equations for URM walls, which are summarised in the following. EC8-Part 3 [4] estimates the drift capacity as a function of the failure mode. According to EC8-Part 3 [4] the "Significant Damage" (SD) drift

Table 4
Summary of failure modes, maximum force capacity, drift at peak load, drift at horizontal failure and maximum drift. The bold values indicate the resulting ultimate drift.

Specimen	Failure mechanism	Axial load ratio σ_0/f_u	Shear span H_0	Peak load A+/− (kN)	Drift at peak load A+/− (%)	Drift at hor. failure B+/− (%)	Maximum drift (%)
PUP1	Diagonal shear	0.18	0.5*H*	187	0.15	0.29	0.31
				−167	−0.12	**−0.17**	−0.21
PUP2	Diagonal shear	0.18	0.75*H*	178	0.35	0.40	0.41
				−164	−0.37	–	**−0.38**
PUP3	Flexural rocking	0.18	1.5*H*	121	0.51	**0.72**	0.84
				−115	−0.72	−0.93	−0.94
PUP4	Hybrid failure	0.26	1.5*H*	145	0.27	**0.35**	0.44
				−142	−0.36	–	−0.38
PUP5	Diagonal shear	0.09	0.75*H*	135	0.37	0.56	0.58
				−121	−0.53	**−0.54**	−0.55
PUP6	Hybrid failure	0.26	1.5*H*	132	0.54	–	0.74
		0.09	0.75*H*	−154	−0.70	–	**−0.71**

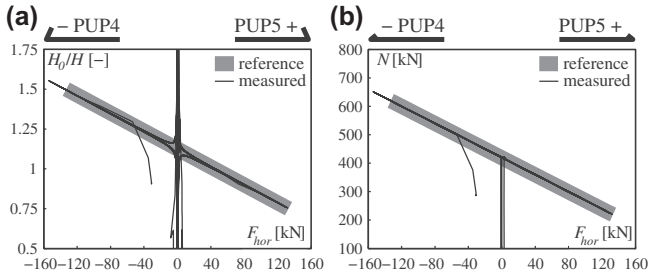

Fig. 12. Shear span ratio and axial load for PUP6 as a function of the applied horizontal load.

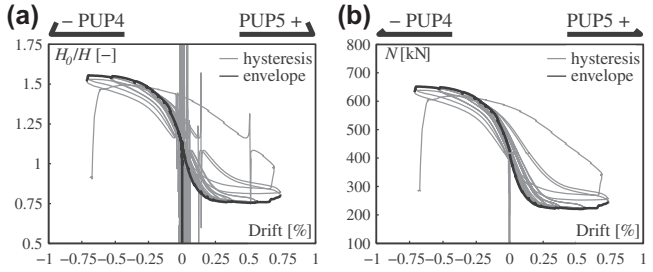

Fig. 13. Shear span ratio and axial load for PUP6 as a function of the applied horizontal drift.

capacity is 0.4% for shear failure and 0.8% H_0/L for flexural failure where L is the length of the wall. The German national annex to EC8 [9] limits the use of 0.4% drift for shear failure for walls with an axial stress ratio of $\sigma_0/f_k \leqslant 0.15$ where f_k is the characteristic compression strength of the masonry. For walls loaded to higher axial stress ratio the SD drift capacity is reduced to 0.3% for shear. The NC drift capacities are estimated as 4/3 times the SD drift capacities: $4/3 \times 0.4\% = 0.53\%$ for shear failure and $4/3 \times 0.8\%$ $H_0/L = 1.07\%$ H_0/L for flexural failure. In EC8-Part 3, the limit state "Near Collapse" (NC) corresponds to a 20% loss of peak strength and therefore to the definition of horizontal load failure adopted in this paper. The Italian code only provides drift limits for the ultimate limit state (ULS) [10]. The shear drift capacity corresponds to the SD limit state drift capacity in EC8-Part 3 but for flexural failure the Italian code provides a fixed drift value of 0.8%, which is hence independent of the slenderness ratio H_0/L [10,11]. The supplement on masonry structures [12] to the New Zealand Standard for seismic assessment [13] proposes ULS drift capacities which are equal to the values in EC8-Part 3 for the SD limit state. The only difference relates to the drift capacity of walls with flanges, which is assumed 50% larger than for walls with a rectangular cross section when failing in shear (0.6% instead of 0.4%).

FEMA 306 [14] distinguishes drift capacities for different damage levels and failure modes. The following drift capacities are specified for the "heavy damage" limit state: For a failure comprising only horizontal cracking due to rocking, FEMA 306 assumes 0.8% H_s/L, where H_s is the free height between two storeys. For a failure mode comprising only sliding along the joints (in form of stair step cracks), FEMA assumes 0.4%. For walls failing due to diagonal cracking no drift capacities but only ductility capacities are specified. For mixed modes comprising toe crushing, flexural cracking and bed joint sliding, FEMA 306 specifies a drift capacity of 1.2% and for mixed modes with flexural cracking and toe crushing only a drift capacity of 0.3%. Both mixed failure modes apply only to squad walls with $L/H_s > 1.25$. Hence, if one stipulates that "heavy damage" corresponds to the SD limit state and neglects the mixed modes, the drift capacities proposed by FEMA 306 [14] are very similar to those in EC8-Part 3 [4]. FEMA 273 [15], a guideline for the seismic rehabilitation of buildings, distinguishes also between shear and flexural failure modes when defining drift capacities. NC limit state drift limits for walls of primary structural importance are 0.4% for shear failure and 0.4% H_s/L for flexural failure. Assuming that $\delta_{NC}/\delta_{SD} = 4/3$, the drift capacities in FEMA 273 are 33% lower than those in EC8-Part 3.

Unlike most codes, the Swiss guideline on the seismic assessment of URM structures SIA D0237 [16] does not estimate the drift capacity as a function of the failure mode but expresses the drift capacity as a function of the axial stress ratio σ_0/f_d, where f_d is the design value of the masonry compressive strength. This approach originates from [3] and was developed to be used in conjunction with the Swiss Masonry code SIA 266 [17], which determines the strength capacity of a masonry wall using stress fields and therefore does not distinguish explicitly between different failure modes. Drift estimates that are independent of the failure mode might also be convenient for vulnerability studies of large building stocks as axial load and shear span ratio can be roughly estimated from the geometry of the building and the SIA D0237 estimates the drift capacity δ_{ULS} at the life safety limit state [16] which can be assumed to correspond approximately to the SD limit state:

$$\delta_{SD} = \delta_0 \cdot \left(1 - \frac{\sigma_n}{f_d}\right) \tag{4}$$

where δ_0 is the drift capacity at zero overburden stress, σ_n is the design value of the normal stress and f_d is the design value of the compressive strength of the masonry. For the life safety limit state, SIA D0237 proposes values of 0.8% if the wall is loaded as a cantilever and 0.4% if the boundary conditions are fixed-fixed. Unlike other codes, it accounts explicitly for the boundary conditions to which the wall is subjected. To compare the predicted values to the

Table 5
Dataset of wall tests.

No	Test Unit	Type	References	L (mm)	T (mm)	H (mm)	H_0/H (–)	h_B (mm)	σ_0 (MPa)	f_u (MPa)	σ_0/f_u (–)	Load. History	Fail. Mech.	δ_u (%)
1	10_1	F	[19,18]	1028	300	1510	1.06[a]	240	0.60	4.00	0.15	C	F	1.71
2	10_2	F	[19,18]	1030	300	1510	1.06[a]	240	1.19	4.10	0.29	C	F	0.66
3	10_3	F	[19,18]	1033	300	1515	1.06[a]	240	0.60	4.00	0.15	C	D	1.31
4	10_4	F	[19,18]	1025	300	1514	1.06[a]	240	1.19	4.10	0.29	C	F	0.85
5	10_5	F	[19,18]	1027	300	1511	1.06[a]	240	1.19	4.10	0.29	C	D	0.83
6	10_6	F	[19,18]	1026	300	1508	1.06[a]	240	0.60	4.00	0.15	C	F	2.32
7	10_7	No	[19,18]	989	300	1513	1.06[a]	237	1.19	4.25	0.28	C	F	0.66
8	10_8	No	[19,18]	987	300	1511	1.06[a]	237	1.19	4.25	0.28	C	F	0.83
9	10_9	No	[19,18]	988	300	1507	1.06[a]	237	1.19	4.25	0.28	C	F	0.97
10	10_10	MP	[19,18]	985	300	1508	1.06[a]	236	1.19	6.26	0.19	C	F	0.66
11	10_11	MP	[19,18]	985	300	1509	1.06[a]	236	1.19	6.26	0.19	C	F	0.78
12	10_12	MP	[19,18]	986	300	1507	1.06[a]	236	1.19	6.26	0.19	C	F	0.66
13	10_13	TG	[19,18]	988	300	1510	1.06[a]	235	1.19	6.26	0.19	C	F	0.40
14	10_14	TG	[19,18]	987	300	1512	1.06[a]	235	1.19	6.26	0.19	C	F	0.61
15	10_15	TG	[19,18]	986	300	1508	1.06[a]	235	1.19	6.26	0.19	C	F	0.58
16	14_1	F	[20,18]	2567	297	1750	1.10[a]	236	0.59	4.21	0.14	C	H	1.37
17	14_2	F	[20,18]	2572	297	1753	1.10[a]	236	1.19	4.10	0.29	C	H	0.57
18	14_3	F	[20,18]	2584	297	1751	1.10[a]	236	0.89	4.05	0.22	C	H	0.77
19	14_4	TG	[20,18]	2482	296	1750	1.10[a]	237	0.95	4.32	0.22	C	S	0.72
20	14_5	TG	[20,18]	2484	296	1750	1.10[a]	237	0.53	2.41	0.22	C	F	1.72
21	14_6	MP	[20,18]	2359	247	1600	1.11[a]	188	0.85	3.86	0.22	C	F	0.72
22	14_7	F	[20,18]	2712	172	1820	1.10[a]	188	2.07	9.41	0.22	C	H	0.33
23	15_5	TG	[21,18]	992	300	1170	1.09[a]	225	0.94	5.53	0.17	C	F	1.42
24	15_6	TG	[21,18]	992	300	1170	1.09[a]	225	1.24	5.64	0.22	C	S	1.57
25	15_7	TG	[21,18]	992	300	1170	1.09[a]	225	1.55	5.74	0.27	C	F	1.58
26	15_8	MP	[21,18]	992	300	1170	1.09[a]	225	0.89	5.24	0.17	C	F	2.91
27	15_9	MP	[21,18]	992	300	1170	1.09[a]	225	1.14	5.18	0.22	C	F	1.98
28	15_10	MP	[21,18]	992	300	1170	1.09[a]	225	1.46	5.41	0.27	C	F	1.37
29	16_1	MP	[18][c]	2500	300	1750	0.50	238	0.40	5.71	0.07	C	S	0.25
30	16_2	MP	[18][c]	2500	300	1750	0.50	238	0.60	6.00	0.10	C	S	0.14
31	16_3	MP	[18][c]	2500	300	1750	0.50	238	0.60	6.00	0.10	C	S	0.24
32	18_1	MP	[18][c]	2500	300	1750	0.50	238	0.60	6.00	0.10	C	S	1.00
33	18_2	MP	[18][c]	2500	300	1750	0.50	238	0.60	6.00	0.10	C	S	1.00
34	18_3	MP	[18][c]	2500	300	1750	0.50	238	0.60	6.00	0.10	C	S	2.00
35	18_4	MP	[18][c]	2500	300	1750	0.50	238	0.60	6.00	0.10	C	S	1.22
36	18_5	MP	[18][c]	2500	300	1750	0.50	238	0.60	6.00	0.10	C	S	1.12
37	18_6	MP	[18][c]	2500	300	1750	0.50	238	0.60	6.00	0.10	C	S	1.00
38	CL04	F	[22,18]	2500	300	2600	0.50	190	0.68	9.71	0.07	C	S	0.34
39	CL05	F	[22,18]	2500	300	2600	0.50	190	0.68	9.71	0.07	C	S	0.25
40	CL06	F	[22,18]	1250	300	2600	0.50	190	0.50	10.00	0.05	C	F	1.95
41	CL07	TG	[22,18]	1250	300	2600	0.50	190	0.50	7.14	0.07	C	S	0.22
42	CL08	TG	[22,18]	2500	300	2600	0.50	190	0.68	6.80	0.10	C	S	0.40
43	W1	F	[23]	3600	150	2000	1.04	190	0.77	8.25	0.09	M	S	0.94
44	W2	F	[23]	3600	150	2000	1.04	190	2.38	8.25	0.29	M	H	0.40
45	W4	F	[23]	3600	150	2000	2.11	190	0.78	8.25	0.09	M	H	1.11
46	W6	F	[23]	3600	150	2000	1.04	190	0.77	8.25	0.09	C	D	0.45
47	W7	F	[23]	3600	150	2000	1.04	190	2.39	8.25	0.29	C	S	0.20
48	MR-A1	MP	[24]	1500	150	1190	1.43[a]	190	1.00	9.40	0.11	C	H	0.51
49	MR-B1	MP	[25]	1800	150	1400	1.36[a]	190	0.50	9.40	0.05	C	F	0.72
50	CM01	F*	[26]	950	120	1400	1.00[b]	65	2.72	14.98	0.18	C	D	0.57
51	CM02	F*	[26]	950	120	1400	1.00[b]	65	2.72	14.98	0.18	C	D	1.11
52	MI1m	F*	[27,28]	1500	150	2000	0.50	55	1.02	7.92	0.13	M	S	0.88
53	MI1	F*	[27,28]	1500	150	2000	0.50	55	1.12	7.92	0.14	C	S	0.51
54	MI2	F*	[27,28]	1500	150	2000	0.50	55	0.68	7.92	0.09	C	S	0.60
55	MI3	F*	[27,28]	1500	150	3000	0.50	55	1.24	7.92	0.16	C	H	0.49
56	MI4	F*	[27,28]	1500	150	3000	0.50	55	0.69	7.92	0.09	C	S	0.50
57	ISP1	F*	[29,28]	1000	250	1350	0.50	55	0.60	6.20	0.10	C	S	0.44
58	ISP3	F*	[29,28]	1000	250	2000	0.50	55	1.08	6.20	0.17	C	F	0.53
59	PUP1	F	EPFL-Test	2010	200	2250	0.50	190	1.05	5.86	0.18	C	S	0.17
60	PUP2	F	EPFL-Test	2010	200	2250	0.75	190	1.05	5.86	0.18	C	S	0.38
61	PUP3	F	EPFL-Test	2010	200	2250	1.50	190	1.05	5.86	0.18	C	F	0.72
62	PUP4	F	EPFL-Test	2010	200	2250	1.50	190	1.54	5.86	0.26	C	H	0.35
63	PUP5	F	EPFL-Test	2010	200	2250	0.75	190	0.55	5.86	0.09	C	S	0.54
64	PUP6	F	EPFL-Test	2010	200	2250	1.55	190	1.54	5.86	0.26	A	S	0.71
	Min			950	120	1170	0.50	55	0.40	2.41	0.05			0.14
	Max			3600	300	3000	2.11	240	2.72	14.98	0.29			2.91

Legend: Type of masonry: F = Hollow clay brick masonry with fully mortared joints, F* = Solid clay brick masonry with fully mortared joints, No = Hollow clay brick masonry with unfilled head joints, MP = Mortar pocket masonry, TG = Tongue and groove masonry (unfilled head joints).
Loading history: C = symmetric cycles, M = monotonic loading, A = asymmetric cycles.
Failure modes: S = Shear failure, F = Flexural failure, H = Hybrid failure, D = Failure mechanism doubtful/unknown.
The data on test units 1–42 was taken from [18]. The first references indicated are the primary references given in [18].
[a] Shear span estimated from drawing or photo of test setup in corresponding reference.
[b] Shear span could not be estimated from corresponding reference.
[c] Primary reference was not specified in [18].

experimental values, δ_{SD} needs to be converted to δ_{NC} and the design values of the masonry strength f_d to the mean strength f_u. For the ratio δ_{NC}/δ_{SD} a value of 4/3 is assumed (EC8-Part 3 [4]). If the probabilistic distribution is not known, EN 1052-1 [6] proposes that the mean strength f_u is 20% larger than the characteristic value. The Swiss masonry code applies a safety factor of $\gamma_M = 2.0$ for transforming the characteristic strength into a design value. Hence, with $f_u = 2.4\, f_d$ and $\delta_{NC} = 4/3\ \delta_{SD}$, Eq. (4) can be rewritten as:

$$\text{Cantilever}: \quad \delta_{NC} = \frac{4}{3} \cdot 0.8 \cdot \left(1 - 2.4\frac{\sigma_0}{f_u}\right) \tag{5}$$

$$\text{Fixed-fixed}: \quad \delta_{NC} = \frac{4}{3} \cdot 0.4 \cdot \left(1 - 2.4\frac{\sigma_0}{f_u}\right) \tag{6}$$

SIA D0237 intended these equations to yield conservative estimates of the drift capacity obtained from quasi-static cyclic tests [16]. They were determined on the basis of a dataset comprising walls of different heights tested as cantilevers or with fixed-fixed boundary conditions.

5.2. Dataset of quasi-static wall tests including PUP-series

The dataset comprises results from quasi-static tests on URM walls constructed with clay brick units and normal cement mortar. All walls were constructed with full-size brick units. Own tests with fully mortared and unfilled head joints as well as results reported in the literature, e.g. [18], suggested that the type of head joints has relatively little influence on the deformation behaviour of masonry walls. For this reason, quasi-static tests on URM walls with fully mortared head joints, unfilled head joints, mortar pocket as well as tongue and groove masonry are considered. Table 5 summarises the dimensions of the walls, the ratio H_0/H, the applied axial stress σ_0, the mean masonry strength f_u, the brick height h_B, the observed failure mode as well as the drift capacity δ_u. The dataset includes in total 64 tests that stem from 13 test series conducted in 8 different structural engineering laboratories.

The information on test units 1–42 is taken from [18]. It collects data on a large variety of masonry wall tests, assesses the failure modes and determines the drift capacity of the walls in a uniform manner. Tests 43–64 were added from different primary sources and include also the six tests PUP1-6 presented in the first part of this paper. The data was processed as in [18]. Thus, the ultimate drift δ_u is determined as the minimum value of the drifts attained at horizontal and vertical load failure. Apart from the PUP-series, all walls were subjected to boundary conditions corresponding either to fixed-fixed or to a cantilever. The ratio H_0/H was therefore for these tests either 0.5 or $\geqslant 1.0$. For the cantilever tests the shear span H_0 was defined as the distance between the centre line of the horizontal actuator and the base of the walls (see Table 5).

5.3. Consideration of loading history and strain rate

During seismic loading, URM walls are subjected to loading histories substantially different to the symmetric cycles with increasing amplitudes applied in most quasi-static tests. Furthermore, the strain rates under seismic loading are much larger than in quasi-static tests. For this reason, drift limits derived from quasi-static cyclic tests (δ_{CT}) should not be adopted directly in code recommendations for δ_{NC} but need to be modified to account for loading history (ψ_{LH}) and strain rate (ψ_{SR}) effects. In the absence of mechanical models that account for these effects in an explicit manner, we propose the following simple relationship to estimate the seismic drift capacity associated with the NC limit state from quasi-static cyclic test results:

$$\delta_{NC} = \delta_{CT} \cdot \psi_{LH} \cdot \psi_{SR} \tag{7}$$

At present, the dataset for determining the correction factor ψ_{SR} is very limited. Abrams and Paulson [31,32] report a more important crack propagation in URM structures when tested quasi-static cyclically than when tested dynamically. However, Tomaževič [33] and Elgawady [34] report similar displacement capacities for masonry walls tested quasi-statically or dynamically suggesting hence $\psi_{SR} = 1$.

With regard to loading history effects (ψ_{LH}) the data is also rather limited: the dataset (Table 5) contains five tests which were not subjected to symmetric cycles. Nevertheless, a comparison between cycles from real seismic loading and symmetric cycles with increasing amplitude is missing. The five tests are PUP6, which was subjected to an asymmetric loading history, and four tests conducted as monotonic tests. For four of these five tests also counterparts subjected to a symmetric cyclic loading history are available and allow to draw first conclusions regarding the effect of the load history: as outlined in Section 4.3, PUP6 can be compared to PUP4 while the counterparts of tests 43, 44 and 52, which had been subjected to monotonic loading, are the cyclic test 46, 47 and 53. Fig. 14 shows that the drift capacity of monotonically or asymmetrically loaded test units is larger than of symmetrically loaded test units. The ratios of drift capacities varied between 1.75 and 2.10. The drift capacity of a monotonically or asymmetrically loaded wall is therefore approximately twice the drift capacity of a cyclically loaded wall. This suggests that ψ_{LH} could be significantly larger than unity. Based on own experience with quasi-static cyclic and shake table tests, we estimate that $\psi_{SR} * \psi_{LH}$ could be in the order of 2–3. Since quasi-static cyclic tests will most likely remain the standard test for URM walls in the future, further research on ψ_{SR} and ψ_{LH} is needed but is out of the scope of this paper.

5.4. Size effect on drift capacity

Empirical drift capacity models, e.g. [16], were developed as best fit lines to datasets similar to the one presented in Table 5. Many of the wall tests documented in the literature were conducted on walls with heights less than a storey. Such walls are present in facades with masonry spandrels while walls at the interior of the building and walls in modern URM buildings typically span over the entire storey height. Assuming a storey height of $H_s = 2.4$ m, out of the 64 test units documented in Table 5, only 7 were conducted on storey-high walls ($H \geqslant 2.4$ m). The next smaller test units are the six test units of the PUP-series, which

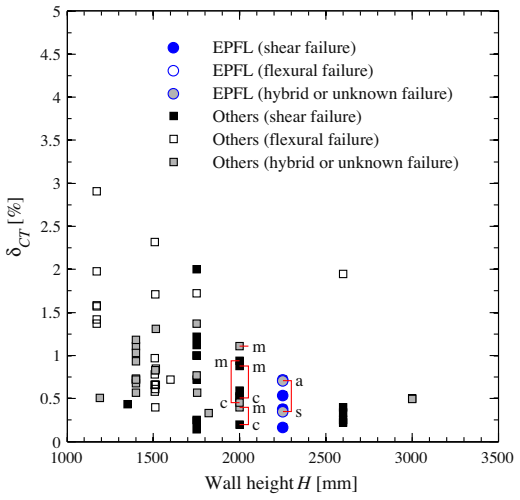

Fig. 14. Drift capacities obtained from quasi-static tests vs height of wall specimens (c = symmetric cyclic tests, a = asymmetric cyclic tests, m = monotonic test).

had a height of 2.25 m ($H = 0.94\ H_s$). 27 test units were conducted with heights smaller than $2/3H_s$.

Including test units of different heights in the dataset when developing simple empirical models has, however, a significant implication: Fig. 14 shows that the experimentally determined drift capacity is strongly dependent on the height of the test unit. Hence, there is a strong size effect on the drift capacity of URM walls, which leads to larger drift capacities for walls of smaller heights. To our knowledge, this effect has been disregarded when developing empirical drift capacity models from experimental results, which might potentially lead to unsafe drift predictions for storey-high walls. The trend in the experimental data agrees, with results of a numerical study by Lourenço [30] who analysed masonry structures at different scales by means of simplified micro models.

Lourenço [30] found that the maximum strength of masonry walls increased as the size of the specimen was reduced. This applied if failure occurred due to tensile failure of bricks or due to crushing of the masonry. For sliding failure, the strength was independent of the size as sliding is a ductile mechanism. For compression failure modes, which are characterised by a softening regime after reaching the peak strength, also the slope of the post-peak branch depended strongly on the size of the test unit: the larger the wall, the steeper the drop in strength after peak strength and thus the smaller the displacement capacity associated with horizontal load failure. Lourenço acknowledged that the adopted modelling approach might not be adequate for capturing correctly compression failure. However, his results are confirmed qualitatively by the experimental data in Fig. 14: most walls subjected to horizontal displacements fail eventually due to crushing of the compression zone or the failure along a diagonal crack passing through bricks. For such failure modes, size effects are expected to play a role. A pure sliding failure, which would not be affected by size effects, is hardly observed. Most failure modes are in fact hybrid modes and depending on the contribution of the different mechanisms, the size effect might influence the drift capacity to different extents. At present, mechanical models that predict the deformation capacity of URM walls are, however, lacking and one must fall back on simple empirical models. To account for the size effect in empirical drift capacity models a height dependent term should be introduced; a simple model including such a term is proposed in Section 5.5.

5.5. Revised empirical relationships for the drift capacity of URM walls

In the following, the coefficients of three different drift capacity models of walls are evaluated from the dataset of Table 5. These are: (i) the model in EC8-Part 3 [4] which distinguishes between failure modes, (ii) the model in SIA D0237 [16] which accounts for the boundary conditions (axial stress ratio and moment profile), and (iii) a new model which introduces a height dependent term to the SIA-model. In accordance with the definition of δ_{CT}, only walls subjected to symmetric cycles are considered.

5.5.1. Drift capacity models based on failure modes (Modified EC8 model)

Fig. 15 plots for three different failure modes (shear, flexural, hybrid/unknown) the experimentally determined drift capacities as a function of the test units' height. For all three failure modes, the drift capacities decrease with the wall height. Based on the cyclic tests of the dataset in Table 5, the 5 and 50% fractile values of the drift capacity of walls of all heights failing in shear and flexure are:

Shear failure (22 test units, Fig. 15a):

$$\delta_{CT,5\%} = 0.14\% \quad \delta_{CT,50\%} = 0.47\%$$

Flexural failure (25 test unit, Fig. 15b):

$$\delta_{CT,5\%} = 0.26\% H_0/L \quad {}_{CT,50\%} = 0.74\% H_0/L$$

Including the slenderness ratio H_0/L does not improve the goodness of fit. It is therefore suggested to omit, as the Italian code does [10,11], the slenderness ratio and to estimate the flexural drift capacity also by a constant value:

Flexural failure (25 test unit):

$$\delta_{CT,5\%} = 0.41\% \quad \delta_{CT,50\%} = 1.00\%$$

The ratios between 5% and 50% fractile values are for shear and flexural failure modes approximately 2.5–3. Assuming a drift ratio $\delta_{NC}/\delta_{SD} = 4/3$ [4] and $\psi_{LH} * \psi_{SR} = 2$–3 one obtains the following drift capacities at the SD limit state:

Shear failure:

$$\delta_{SD,5\%} \simeq 0.20\text{—}0.30\% \quad \delta_{SD,50\%} \simeq 0.70\text{—}1.05\%$$

Flexural failure:

$$\delta_{SD,5\%} \simeq 0.60\text{—}0.90\% \quad \delta_{SD,50\%} \simeq 1.50\text{—}2.25\%$$

The values were rounded to the nearest 0.05. The 5% fractile values are slightly smaller than the drift capacities proposed in EC8-Part 3 [4], which would correspond for the assumed correction factors to 10–30% fractile values of the dataset in Table 5.

5.5.2. Drift capacity model based on boundary conditions (Modified SIA-model)

To generalise the effect of the shear span on the wall's drift capacity, Eqs. (5) and (6) are condensed into:

$$\delta_{CT} = \delta_0 \cdot \left(1 - \alpha \frac{\sigma_0}{f_u}\right) \cdot \frac{H_0}{H} \tag{8}$$

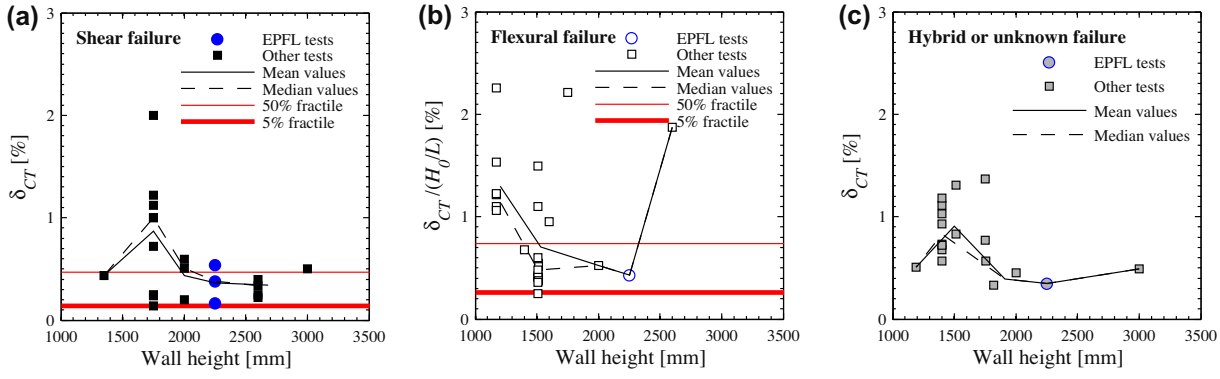

Fig. 15. Modified EC8 – Part 3: Comparison of best-fit drift capacities to drift capacity obtained from quasi-static tests on walls with different heights.

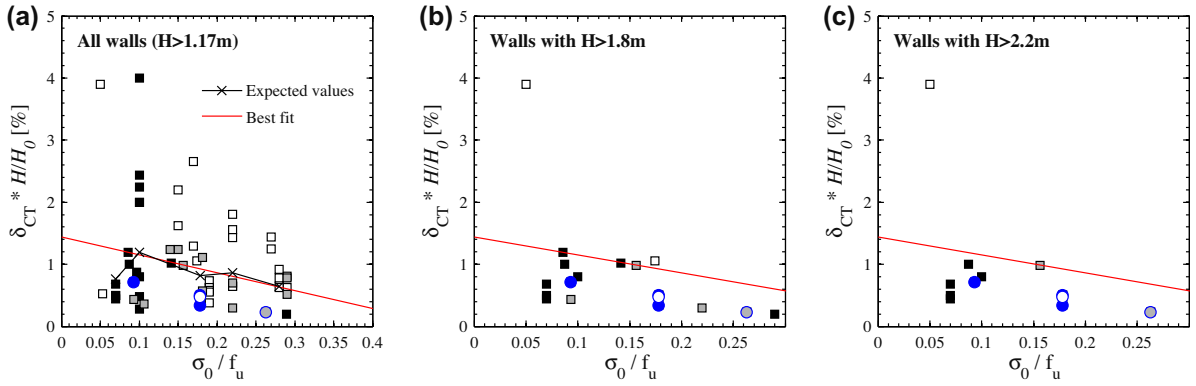

Fig. 16. Modified SIA-model: Comparison of best-fit drift capacities to drift capacities obtained from quasi-static cyclic tests on walls with different heights.

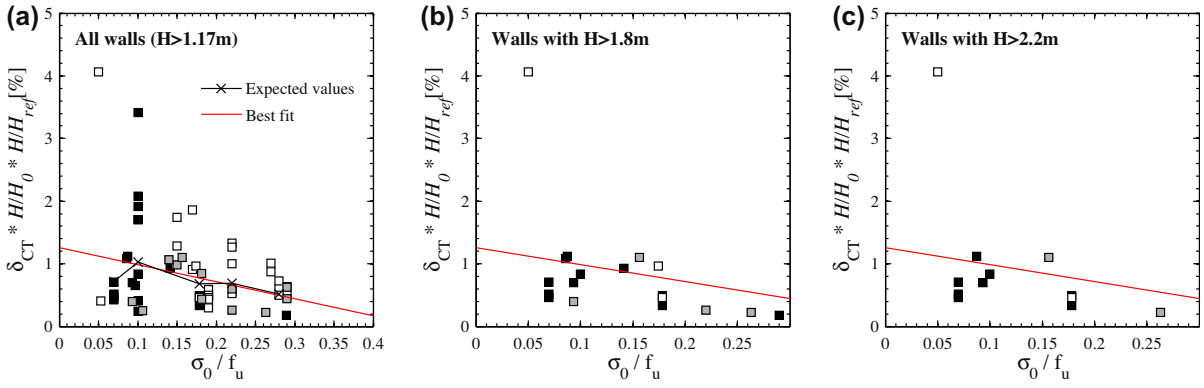

Fig. 17. New-model: Comparison of best-fit drift capacities to drift capacities obtained from quasi-static cyclic tests on walls with different heights.

The best fit line obtained for the dataset of Table 5 yields the following coefficients:

$$\delta_{CT,50\%} = 1.45\% \cdot \left(1 - 2.0\frac{\sigma_0}{f_u}\right) \cdot \frac{H_0}{H} \tag{9}$$

Eq. (9) should only be applied to test units with $0.07 \leqslant \sigma_0/f_u \leqslant 0.30$ and $0.5 \leqslant H_0/H \leqslant 1.5$. Assuming again a lognormal distribution of the drift capacities, the values should be divided by 3.0 if 5%-fractile values of the drift capacity are sought. The best fit line was obtained as follows: (i) the drift capacities $\delta_{CT} * H/H_0$ were plotted against σ_0/f_u and the data points grouped in intervals of $0.05\sigma_0/f_u$; (ii) for tests within one interval, the drift values were assumed lognormally distributed and independent of σ_0/f_u (the expected drift value was determined for each interval); (iii) Eq. (9) is the linear approximation of these expected drift values. Fig. 16a shows for the entire dataset the expected values of the σ_0/f_u intervals and the best fit line (Eq. (9)). When compared to two subsets including walls with $H \geqslant 1.8$ m and $H \geqslant 2.2$ m, respectively (b, c), Eq. (9) overestimates the drift capacity but one can also note that the scatter reduces considerably as walls of smaller height intervals are considered. Note that the data for $H \geqslant 2.2$ m walls comprises all three failure modes and test data from three different types of masonry typologies, i.e., hollow clay brick masonry, solid clay brick masonry and tongue and groove masonry (F, F*, TG). The results presented in Fig. 16 underscore that the drift capacity should decrease with increasing wall height (Section 5.4).

5.5.3. Drift capacity model based on boundary conditions and size effect (New model)

In order to account for the decreasing drift capacity with increasing height, an additional term is introduced into Eq. (9).

$$\delta_{CT} = \delta_0 \cdot \left(1 - \alpha\frac{\sigma_0}{f_u}\right) \cdot \frac{H_0}{H} \cdot \left(\frac{H_{ref}}{H}\right)^{\beta} \tag{10}$$

Ideally, the form and coefficients of the term accounting for size effect should be derived from a mechanical model. In the absence of the latter, this simple form is chosen: the coefficient β set to 0.5 and H_{ref} to a constant value of 2400 mm. The best-fit line is computed as outlined in the previous section and the following coefficients are obtained:

$$\delta_{CT,50\%} = 1.3\% \cdot \left(1 - 2.2\frac{\sigma_0}{f_u}\right) \cdot \frac{H_0}{H} \cdot \left(\frac{H_{ref}}{H}\right)^{0.5} \tag{11}$$

When compared to the two subsets (walls with $H \geqslant 1.8$ m and $H \geqslant 2.2$ m), Eq. (11) yields reasonable approximations of the expected drift capacities although it was calibrated on the entire dataset (Fig. 17a). Assuming again a lognormal distribution of the drift capacities, the values should be divided by 2.8 if 5%-fractile values of the drift capacity are sought. For a drift ratio $\delta_{NC}/\delta_{SD} = 4/3$, $\psi_{LH} * \psi_{SR} = 2–3$ and $f_u = 2.4\, f_d$ one obtains as drift limits for the SD limit state:

$$\delta_{SD,5\%} = (0.7\% \div 1.0\%) \cdot \left(1 - 0.9\frac{\sigma_0}{f_d}\right) \cdot \frac{H_0}{H} \cdot \left(\frac{H_{ref}}{H}\right)^{0.5} \tag{12}$$

Fig. 18 shows the ratio of predicted to observed drift capacities. It is clear that the uncertainty remains also for the new model considerable. However, noticeable trends of the ratio of observed to predicted drift capacities with σ_0/f_u and wall height have been eliminated.

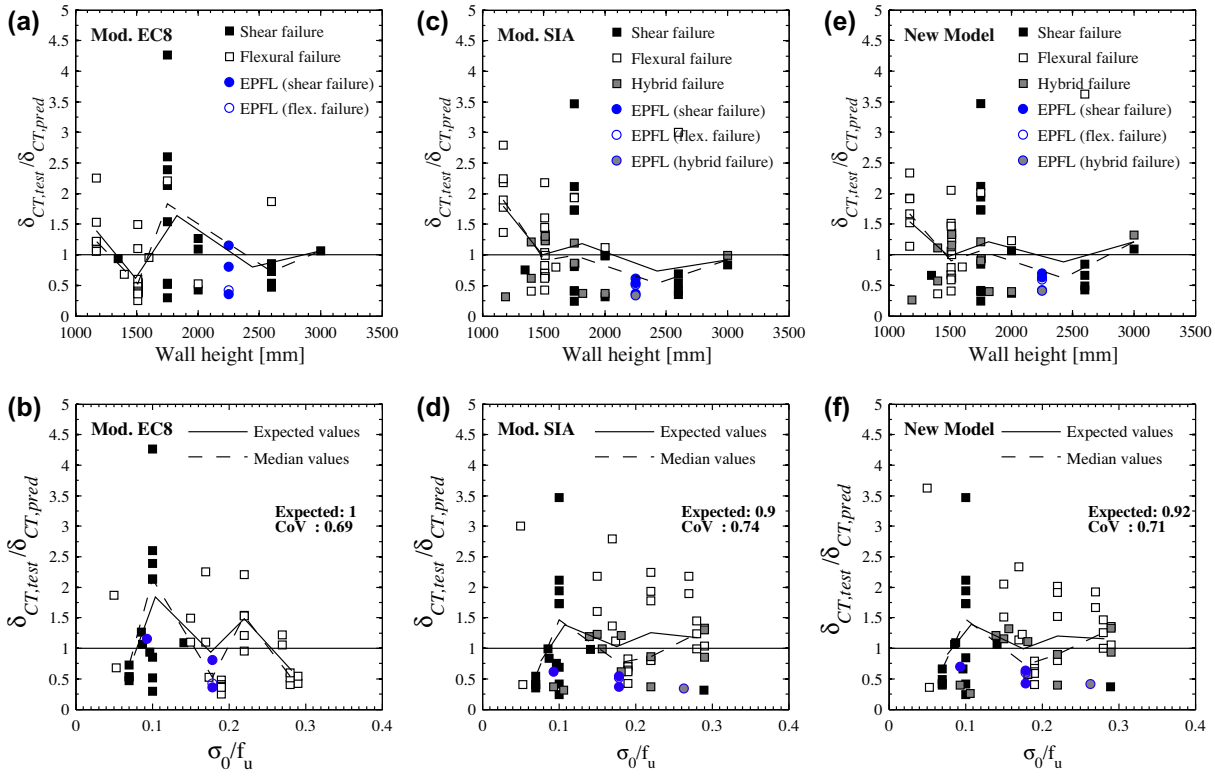

Fig. 18. Ratio of predicted to observed drift ratios for (a, b) modified EC8 model (Shear failure: $\delta_{CT,50\%}$ = 0.47%, Flexural failure: $\delta_{CT,50\%}$ = 1.00%), (c, d) modified SIA model (Eq. (9)) and (e, f) the new model (Eq. (11)).

6. Conclusions

In a first part, the paper presents results of six quasi-static cyclic tests on URM walls which investigated the effect of the boundary conditions on the deformation behaviour of URM walls. The boundary conditions were characterized in terms of applied axial load ratio and moment restraint provided at the top of the wall, which was expressed in terms of the shear span. The results showed that the larger the axial load ratio or the smaller the shear span, the smaller the drift capacity of URM walls. For larger axial load ratios, shear cracks tended to pass through bricks rather than joints leading to faster strength degradation and hence, to a smaller drift capacity of the walls. For a smaller shear span, the contribution of the flexural deformations of the masonry, which result from the opening of horizontal joints, was significantly reduced, resulting in a smaller total drift capacity of the walls.

In the second part of the paper a dataset comprising the results of 64 quasi-static tests on URM walls was analysed. This dataset confirmed the trends observed with regard to the boundary conditions from the first part of the paper. The analysis of the dataset showed further the importance of size effects on the deformation capacity of URM walls: with increasing test unit size, the drift capacity of the walls reduced. Empirical estimates of drift capacities that are included in today's codes do not account for this effect and drift capacity models are independent of the wall's height (e.g. [16]). As a result, when applied to storey-high walls, drift capacities are overestimated.

For seismic analysis of URM structures, a new drift capacity model was proposed, which consists of three components: A drift capacity δ_{CT} derived from quasi-static cyclic tests and two correction factors – ψ_{SR} and ψ_{LH} – accounting for loading history and strain rate effects. Determining the two correction factors was out of the scope of this article and significant further research is required; as a first rough value we estimate from own tests a value of 2–3 for $\psi_{SR} * \psi_{LH}$. For δ_{CT} a new model accounting for boundary conditions (axial load ratio and moment profile) and size effects was proposed. Unlike previous models (EC8-Part 3 [4], SIA D0237 [16]), this model reflects the reduced drift capacity with the increasing wall height. For the time being, this size effect is only accounted by means of the simple term $(H_{ref}/H)^{0.5}$, which lacks a sound justification. H_{ref} is a reference height and is for the time being set equal to a typical storey height (H_{ref} = 2400 mm). Future research should aim at developing a mechanical model for the drift capacity of URM walls, which allows deriving the parameters controlling the size effect. Furthermore, an improved link between drift capacities obtained from quasi-static cyclic tests and drift capacities attained during real seismic loading must be established.

Acknowledgments

The authors would like to thank the three reviewers for their comments that helped to improve the quality and increase the scope of the paper. The authors also thank Morandi Frères SA for the donation of the bricks and the staff of the structural engineering laboratory at EPFL for the support during testing.

References

[1] Lagomarsino S, Penna A, Galasco A, Cattari S. TREMURI program: an equivalent frame model for the nonlinear seismic analysis of masonry buildings. Eng Struct 2013;56:1787–99.
[2] Tomaževič M. Earthquake-resistant design of masonry buildings, series on innovation in structures and construction, vol. 1. London, UK: Imperial College Press; 1999.
[3] Lang K. Seismic vulnerability of existing buildings. Doctoral thesis. Zurich, Switzerland: ETH Zurich; 2002.

[4] Eurocode 8: Design of structures for earthquake resistance – Part 3: General rules, seismic actions and rules for buildings, Design Code EN 1998-3, European Comittee for Standardisation (CEN), Brussels, Belgium; 2005.
[5] Penna A, Lagomarsino S, Galasco A. A nonlinear macroelement model for the seismic analysis of masonry buildings. Earthquake Eng Struct Dynam 2014;43(2):159–79. http://dx.doi.org/10.1002/eqe.2335.
[6] EN 1052-1. Methods of test for masonry. Part 1: Determination of compressive strength, Code EN 1052-1:1998-12. European Committee for Standardisation (CEN), Brussels, Belgium; 2002.
[7] EN 1052-3. Methods of test for masonry. Part 3: Determination of initial shear strength, Code EN 1052-3:2002-10. European Committee for Standardisation (CEN), Brussels, Belgium; 2007.
[8] RILEM TC 76-LUM. Diagonal tensile strength tests of small wall specimens. RILEM Publications SARL; 1991.
[9] National Annex – Nationally determined parameters – Eurocode 8. Design of structures for earthquake resistance – Part 1: General rules, Seismic actions and rules for buildings, National Annex of Germany, DIN EN 1998-1/NA: 2011-01. Berlin, Germany; 2011.
[10] NTC 2008. Decreto Ministeriale 14/1/2008: Norme tecniche per le costruzioni. Ministry of Infrastructures and Transportations, G.U.S.O. n.30 on 4/2/2008; 2008 [in Italian].
[11] MIT, Ministry of Infrastructures and Transportation, Circ. C.S.Ll.Pp. No. 617 of 2/2/2009: Istruzioni per l'applicazione delle nuove norme tecniche per le costruzioni di cui al Decreto Ministeriale 14 Gennaio 2008. G.U. S.O. n. 27 of 26/2/2009, No. 47; 2008 [in Italian].
[12] NZSEE: Assessment and improvement of unreinforced masonry buildings for earthquake resistance. In: Ingham J, editor. New Zealand Society of Earthquake Engineering, Supplement to Assessment and improvement of the structural performance of buildings in earthquakes. University of Auckland, New Zealand; 2011.
[13] NZSEE: Assessment and improvement of the structural performance of buildings in earthquakes. New Zealand Society of Earthquake Engineering. University of Auckland, New Zealand; 2006.
[14] ATC, FEMA-306: Evaluation of earthquake damaged concrete and masonry wall buildings. Basic Procedures Manual, Applied Technology Council (ATC), Washington, DC, USA; 1998.
[15] ATC, FEMA-273: NEHRP Guidelines for the seismic rehabilitation of buildings. Basic procedures manual, applied technology council (ATC), Washington, DC, USA; 1997.
[16] SIA, SIA D0237: Evaluation de la sécurité parasismique des bâtiments en maçonnerie. Documentation, Swiss Society of Engineers and Architects SIA, Zürich, Switzerland; 2011 [in French].
[17] SIA, SIA 266: Masonry. Swiss code, Swiss society of engineers and architects SIA, Zürich, Switzerland; 2005.
[18] Frumento S, Magenes G, Morandi P, Calvi GM. Interpretation of experimental shear tests on clay brick masonry walls and evaluation of q-factors for seismic design. Technical report, IUSS PRESS, Pavia, Italy; 2009.
[19] Bosiljkov V, Tomaževič M. Test Report, ZAG Ljubljana, Slowenia; 2003.
[20] Bosiljkov V, Tomaževič M. Optimization of shape of masonry units and technology of construction for earthquake resistant masonry buildings. Research Report – part three, ZAG Ljubljana, Slowenia; 2006.
[21] Modena F, Da Porto F, Garbin F. Ricerca sperimentale sul comportamento di sistemi per muratura portante in zona sismica, Draft 2005/01, University of Padua, Italy; 2005 [in Italian].
[22] Magenes G, Morandi P, Penna A. Enhanced safety and efficient construction of masonry structures in europe – d 7.1c test results on the behaviour of masonry under static cyclic in plane lateral loads. Report ESECMaSE D7.1c. University of Pavia, Pavia, Italy; 2008.
[23] Ganz HR, Thürlimann B. Versuche an Mauerwerksscheiben unter Normalkraft und Querkraft. Test Report 7502-4, ETH Zürich, Switzerland; 1984 [in German].
[24] Suter R, Broye A, Grisanti M. Essais de cisaillement de murs en maçonnerie renforces – Série expérimentale MR-A. Report Projet de recherche AGP 21'159, Ecole d'ingénieurs et d'architectes de Fribourg, Fribourg, Switzerland; 2010 [in French].
[25] Suter R, Grisanti M. Essais de cisaillement de murs en maçonnerie renforces – Série expérimentale MR-B. Report Projet de recherche AGP 21'159, Ecole d'ingénieurs et d'architectes de Fribourg, Fribourg, Switzerland; 2010 [in French].
[26] Bosiljkov V, Page AW, Bokan-Bosiljkov V, Zarnic R. Performance based studies of in-plane loaded unreinforced masonry walls. Masonry Int 2003;16(2):39–50.
[27] Magenes G, Calvi GM. Cyclic behaviour of brick masonry walls. In: Proceedings of the 10thworld conference on earthquake engineering, Madrid, Spain; 1992. p. 3517–22.
[28] Magenes G, Calvi GM. In-plane seismic response of brick masonry walls. Earthquake Eng Struct Dynam 1997;26:1091–112.
[29] Anthoine A, Magenes G, Magonette G. Shear compression testing and analysis of brick masonry walls. In: Proceedings 10th European conference on earthquake engineering, Vienna, Austria; 1994. p. 1657–62.
[30] Lourenço PB. Two aspects related to the analysis of masonry structures: Size effect and parameter sensitivity. Technical report TU-DELFT No 03.21.1.31.25/TNO-BOUW No 97-NM-R1533. Faculty of Engineering, TU Delft, Netherlands; 1997.
[31] Abrams D. Effects of scale and loading rate with tests of concrete and masonry structures. Earthq Spectra 1996;12(1):13–28.
[32] Paulson TJ, Abrams D. Correlation between static and dynamic response of model masonry structures. Earthq Spectra 1990;6(3):573–91.
[33] Tomaževič M. Some aspects of experimental testing of seismic behaviour of masonry walls and models of masonry buildings. ISET J Earthq Technol 2000;37(4):101–17.
[34] Elgawady M. Seismic in-plane behavior of URM walls upgraded with composites. PhD thesis. Lausanne, Switzerland: EPF Lausanne; 2004.